Electron transfer in Li^+-doped Zn-Porphyrin–[10]CPP⊃Fullerene junction. Charge-separated bands with opposite response to polar environment

A. J. Stasyuk,*[a] O. A. Stasyuk,[a] M. Solà*[a] and A. A. Voityuk*[a,b]

a. Institut de Química Computacional and Departament de Química, Universitat de Girona, C/ Maria Aurèlia Capmany 69, 17003 Girona, Spain.

b. Institució Catalana de Recerca i Estudis Avancats (ICREA), 08010 Barcelona, Spain.

Abstract

Recently synthesized porphyrin–cycloparaphenylene (ZnP-[10]CPP) junction is a powerful platform to develop useful organic photovoltaic devices. In this work, we computationally study photoinduced electron transfer processes in the supramolecular complex ZnP–[10]CPP⊃C_{60} and its Li^+-doped derivative. The most striking finding is charge separation (CS) bands in ZnP–[10]CPP⊃Li^+@C_{60} with opposite responses to solvent polarity. Besides CS that demonstrate a bathochromic shift, there exist CS transitions showing a rarely observed hypsochromic shift. The rates of energy transfer, electron transfer, and charge recombination in the supramolecular complexes are computed by using the semi-classical approach. These estimates suggest that the both types of CS states can be efficiently populated in polar media by decay of locally excited states.

Introduction

A proper combination of donor (D) and acceptor (A) units is the main challenge in the development of photovoltaic systems where long-lived charge-separated (CS) states are generated with a high quantum yield.[1-3] Effective communication between D and A can dramatically influence the dynamics of

photoinduced electron transfer (PET).[4,5] This communication is mainly determined by the nature of a molecular spacer between the D and A sites. That is why D-A systems assembled *via* non-covalent interactions and devoid of spacer are of interest. On the other hand, it is extremely difficult to produce non-covalent complexes with a high structural and functional tunability.[6,7] Finally, the long-term structural stability of a photovoltaic system is also important. To meet these requirements, a series of macrocyclic host molecules such as γ-cyclodextrin,[8-10] butylcalix[8]arene,[11,12] and cycloparaphenylenes (CPP)[13-17] have been designed for C_{60}, and the corresponding host-guest molecular systems have been obtained.

Very recently Y. Xu *et al.* reported a synthesis of supermolecular junctions of Zn-Porphyrin–[10]CPP with different fullerenes, for which photoinduced electron transfer was observed from Zn-Porphyrin (ZnP) to the fullerene.[18] A well defined spatial separation of the donor and acceptor units and modularity of the structure distinguish this complex from the conventional porphyrin–fullerene conjugates.[19-24] The formation of a metastable CS state $(ZnP–[10]CPP)^{+\cdot}(C_{60})^{-\cdot}$ with absorption maximum located in the near-IR range at 1090 nm was detected in femtosecond pump-probe experiments. It was also found that a decrease of solvent polarity, by passing from benzonitrile to toluene, prevents the formation of the CS state and leads to a triplet excited state of C_{60} with absorption at 750 nm. Among several synthesized systems, the complex with pristine C_{60} (ZnP-[10]CPP⊃C_{60}) has the strongest binding constant, $(1.6\pm0.1)\cdot10^6$ L/mol in toluene[18] similar to that measured for the complex [10]CPP⊃C_{60}, $(2.79\pm0.03)\times10^6$ L/mol.[25] Note that the covalent functionalization of the [10]CPP by Zn-Porphyrin fragment affects only slightly the stability of the complex.

Herein we report a comprehensive analysis of photoinduced charge separated states in ZnP–[10]CPP⊃C_{60} and its Li-doped derivative ZnP–[10]CPP⊃Li^+@C_{60}. It is based on Time-Dependent DFT calculations coupled with conductor-like polarizable continuum model (CPCM) to account for environmental effects. The computational results are in a perfect agreement with experimental data for ZnP–[10]CPP⊃C_{60}. In the ZnP–[10]CPP⊃Li^+@C_{60} complex, two types of CS states are predicted: CS_1 formed due to electron transfer

(ET) from [10]CPP unit to C_{60}, and CS_2 resulted from ET between ZnP to C_{60}. The CS states show opposite behavior towards solvation. CS_2 is strongly stabilized, whereas CS_1 is destabilized with increasing solvent polarity.

Stability and ground state properties.

The ground state (GS) geometries of ZnP–[10]CPP⊃C_{60} and ZnP–[10]CPP⊃Li^+@C_{60} (Figure 1) were optimized using BLYP-D3(BJ)/def2-SVP scheme.[26-28] Then, excited states were computed using time-dependent DFT formalism with the range-separated CAM-B3LYP[29] functional (see SI for computational details). For the ZnP–[10]CPP⊃C_{60} system, the binding energy (E_B) of C_{60} is -55.1 kcal/mol. The doped system ZnP–[10]CPP⊃Li^+@C_{60} shows a superadditive stabilization effect that leads to a dramatic increase of the binding energy (E_B = -94.6 kcal/mol). For details see Table S1, SI. This effect of Li^+ is similar to that previously reported for carbon nano-onions and other carbon-rich complexes.[30-32]

As seen from Figure 1, the energy band gap in the undoped complex is 3.67 eV, with HOMO localized on the ZnP unit and LUMO on C_{60}. Insertion of Li^+ does not change the HOMO and LUMO localization but substantially affects the gap. Noteworthy is that the orbital energies of HOMO and LUMO change differently. The LUMO energy decreases by 2.88 eV, whereas a decrease of the HOMO energy is rather small, 0.70 eV. More details are given in Table S2, SI. In order to understand this difference, let us look at the charge distribution in both complexes. ZnP–[10]CPP⊃C_{60} has two neutral parts ZnP–[10]CPP and C_{60}. Inserting Li^+ into C_{60} leads to some charge transfer (+0.15 e) from Li^+@C_{60} to ZnP–[10]CPP. In $[Li@C_{60}]^{+0.85}$, the positive charge is mainly localized on Li. The observed changes in the orbital energies can be explained by the electrostatic potential created by Li^+. The HOMO and LUMO energy shifts correlate well with the inverse distance between Li^+ and the fragment where the orbitals are localized. The distance from Li^+ to C_{60} and ZnP is about 3.5 Å and 21 Å, respectively.

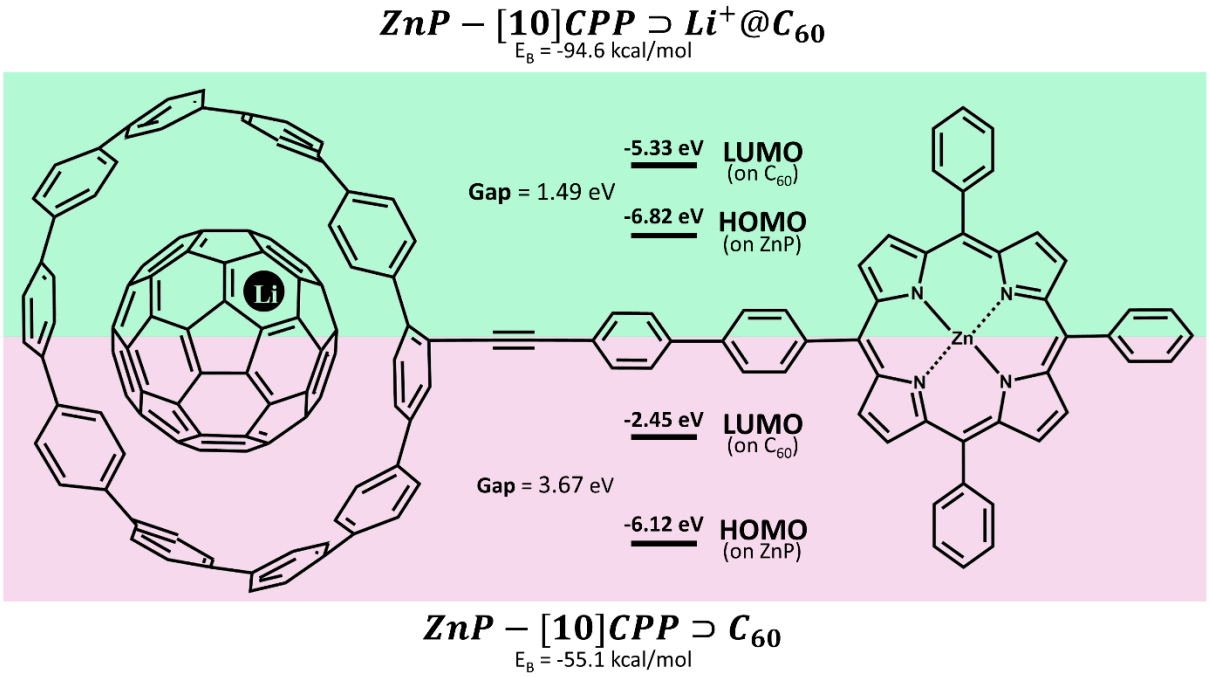

Figure 1. Complexes ZnP–[10]CPP⊃C_{60} (rose, bottom) and ZnP–[10]CPP⊃Li^+@C_{60} (green, top): HOMO and LUMO energies and their localization.

Singlet excited states

For convenience let us divide the complex ZnP–[10]CPP⊃C_{60} into 3 fragments ZnP; [10]CPP; and C_{60}. For ZnP–10CPP⊃Li^+@C_{60}, there is an additional fragment Li^+ (see Figure S1 in SI). Delocalization of exciton and charge transfer contributions were analyzed for 80 lowest excited states of each system. Three types of excited states are identified: locally excited states (LE) with the exciton mainly localized on a single fragment; CS states where electron density (> 0.9e) is transferred between fragments and mixed states with significant contributions of LE and CS (charge separation is between 0.1e and 0.9e). The LE states can be localized on ZnP (LE_1), [10]CPP (LE_2), or C_{60} (LE_3). Two types of CS states are of interest CS_1 states resulted from ET from [10]CPP to C_{60} and CS_2 states generated by ET from ZnP to C_{60}. LE_1 and LE_2 states decay in CS_2 and CS_1, correspondingly, whereas the LE_3 states may yield both CS_1 and CS_2. The analysis of

the excited states is presented in Table 1. In the gas phase, 80 vertical excitation energies of ZnP–[10]CPP⊃C_{60} are in the range from 2.3 to 4.3 eV.

Table 1. Singlet excitation energy (E_x, eV), main singly excited configuration and its weight (W), oscillator strength (f), the contribution of charge separation (CS) and local excitation (X) computed in vacuo and in benzonitrile (BZN).

	Supramolecule			
	ZnP–[10]CPP⊃C_{60}		ZnP–[10]CPP⊃Li^+@C_{60}	
	in vacuo	BZN	in vacuo	BZN
	LE_1 (ZnP)			
E_x	2.338	2.314	2.311	2.308
Transition (W)	H – L+3 (0.54)	H – L+3 (0.56)	H – L+18 (0.47)	H – L+18 (0.58)
f	0.034	0.052	0.063	0.082
X	0.998	0.998	0.992	0.991
	LE_2 ([10]CPP)			
E_x	3.392	3.379	3.411*	3.305*
Transition (W)	H-2 – L+5 (0.34)	H-2 – L+5 (0.36)	H-3 – L+7 (0.21)	H-3 – L+7 (0.15)
f	0.450	0.445	0.374	0.490
X	0.813	0.890	0.259	0.342
	LE_3 (Fullerene C_{60})			
E_x	2.507	2.498	2.487	2.523
Transition (W)	H-5 – L+2 (0.54)	H-5 – L+2 (0.63)	H-22 – L (0.67)	H-22 – L (0.76)
f	< 0.001	< 0.001	< 0.001	< 0.001
X	0.998	0.950	0.914	0.897
	CS_1 ([10]CPP → Fullerene C_{60})			

E_x	2.739	2.528	1.737	1.964
Transition (W)	H-2 – L (0.94)	H-2 – L (0.95)	H-2 – L (0.59)	H-2 – L (0.64)
f	0.001	0.002	0.002	0.006
CS	0.98	0.98	0.98	0.99
	CS_2 (ZnP $\rightarrow$ Fullerene C_{60})			
E_x	3.448	1.274	1.041	0.581
Transition (W)	H-1 – L (0.99)	H-1 – L (0.99)	H – L (0.99)	H – L (1.00)
f	<0.001	0.001	0.001	0.001
CS	1.00	1.00	1.00	1.00

* - mixed state with significant contributions of LE and CS.

LE states. The lowest LE state in ZnP–[10]CPP⊃C_{60} is localized on ZnP and corresponds to a HOMO $\rightarrow$ LUMO+3 transition. The next LE state is localized on C_{60} and lies 0.16 eV higher. This state can be described as HOMO-5 $\rightarrow$ LUMO+2. LE states on [10]CPP are rather high in energy and can be found at 3.39 eV. The LE states in ZnP–[10]CPP⊃Li^+C_{60} are of similar energy (Table 1). However, the difference in LE_2 states needs to be mentioned. In ZnP–[10]CPP⊃Li^+C_{60}, there is no pure LE localized on [10]CPP, only states with significant contributions of LE and CT are found. LE_2 with maximal exciton localization (χ=0.26 in vacuo and 0.34 in BZN) is presented in Table 1. Highly absorptive LE states are localized on the ZnP and C_{60} fragments. Absorption spectra simulated for both complexes are shown in Figure S2, SI. LE states with high oscillator strength localized on [10]CPP in ZnP–[10]CPP⊃Li^+C_{60} are not detected within 120 computed excited states.

CS states. The lowest CS_1 state, E_x = 2.74 eV, in the neutral complex, ZnP–[10]CPP^+⊃C_{60}^-, generated by ET (0.98*e*) between [10]CPP and C_{60}. The CS_2 state is about 0.70 eV higher in energy (Ex = 3.45 eV), and corresponds to ET from ZnP to C_{60}. Insertion of Li^+ into ZnP–[10]CPP⊃C_{60} leads to significant changes in

the energetics of CS states. The energy of CS_1 decreases by nearly 1 eV. The effect is more pronounced for CS_2 state with an energy decrease of 2.40 eV. The remarkable difference is due to the electrostatic potential created by Li^+ on the fragments. A large distance between ZnP and Li^+ (∼21 Å) leads to a relatively small shift of HOMO (by about 0.70 eV, see Fig. 1), whereas a dramatic energy shift (by 2.88 eV) of LUMO (localized on C_{60} is associated with the small distance of 3.5 Å between C_{60} and Li^+. The distance from Li^+ to [10]CPP is about 7 Å, which shifts the LUMO on [10]CPP by 2.33 eV . Thus, the Li^+ encapsulation reduces the HOMO-LUMO gap for ZnP - C_{60} by 2.18 eV and the gap for [10]CPP - C_{60} by 0.55 eV. The different response of the CS states to the Li^+ encapsulation results in qualitative changes in the ET picture: the lowest CS state in the initial (neutral) complex is formed by ET between CPP and C_{60} whereas it becomes ZnP^+–C_{60}^- in the doped system. The relevant frontier molecular orbitals are shown in Figure S3 and S4.

Environment effects

To evaluate the effect of solvation on the excited states, a well established COSMO-like model[33-36] was applied with benzonitrile (BZN) as a solvent. The GS solvation energies for ZnP–[10]CPP⊃C_{60} is found to be -0.26 eV. The solvation energy of the charged complex ZnP–[10]CPP⊃Li^+@C_{60} is noticeably larger, -1.38 eV. Usually, changes in the solvation energies for LE excitations are relatively small, while CT transition are more sensitive to polar medium.[37] These solvation effects correlate with a change of the dipole moment by excitation. Interesting features were observed for CS_1 and CS_2 states, ZnP–[10]CPP$^{+\cdot}$⊃$C_{60}^{-\cdot}$ and $ZnP^{+\cdot}$– [10]CPP⊃$C_{60}^{-\cdot}$, in the neutral complex. The difference in the dipole moments in the GS and CS_1 states is only 1.4D, which is due to a short distance between the involved fragments and even charge delocalization. A relative solvation energy of CS_1 (compared to GS) is equal to 0.21 eV (Table 1). This stabilization is insufficient to reorder the CS_1 and LE states when passing from the gas phase to a highly polar BZN solution. In contrast, a strong solvent stabilization of the CS_2 state, -2.17 eV, was found. The difference in the GS and CS_2 dipole moments is larger than 100 D because of a large distance (~ 21 Å) between ZnP^+ and $C_{60}^{-\cdot}$. This makes the CS_2 state to be the lowest-lying excited state that can be populated

by decay of the LE state. These results are in perfect agreement with spectroscopic measurements made by Y. Xu *et al.*[18] Time-resolved transient absorption spectroscopy indicated that a fast decay of the porphyrin LE goes together with a growth of absorption maximum in the near-IR range at 1090 nm (1.14 eV). This band was attributed to the absorption of the one-electron reduced form of C_{60}.[38,39] The close to each other calculated and experimental values (1.27 vs 1.14 eV) indicate that the chosen computational method suits well for the considered systems.

In our previous work, it was demonstrated that photoinduced CS states in the [10]CPP⊃Li^+@C_{60} complex exhibit a reverse solvent effect, blue shift of CT band by polar medium.[32] A similar behavior is observed for the CS_1 state in ZnP–[10]CPP⊃Li^+@C_{60}. By passing from the gas-phase to the polar BZN solution, a hypsochromic shift of 0.23 eV is detected. In contrast, CS_2 state is strongly stabilized by BZN resulting in the bathochromic shift of the absorption band by 0.46 eV, which is essentially smaller than the stabilization energy of CS_2 (2.17 eV) in the neutral ZnP–[10]CPP⊃C_{60}. To explain this difference, let us compare the CS_2 state in both complexes. In the neutral complex, both fragments $ZnP^{+\cdot}$ and $C_{60}^{-\cdot}$ are charged and the total solvation energy is large. In ZnP–[10]CPP⊃Li^+@C_{60} the fragment Li^+@$C_{60}^{-\cdot}$ is almost neutral, and its solvation energy small. In this case, the total solvation energy is determined mainly by the contribution of $ZnP^{+\cdot}$.

To gain a better insight, we performed excited state calculation in several additional solvents with the dielectric constant ε ranging from 2.4 (toluene) to 8.9 (dichloromethane). As seen from Figure 2, the solvation energy of the LE_1 and LE_3 states (black lines) in both ZnP–[10]CPP⊃C_{60} and ZnP–[10]CPP⊃Li^+@C_{60} does not depend on the solvent polarity. The CS_2 state in both complexes is strongly stabilized by polar environment, while its energy in the neutral complex is more sensitive. In contrast, the CS_1 state in neutral and Li^+-doped systems has a comparable response to the solvent polarity but shows the opposite trend (blue lines in Figure 2). In ZnP–[10]CPP⊃C_{60}, the CS_1 excitation exhibits a bathochromic shift (Figure 2, left

panel) although a hypsochromic shift of the absorption band (Figure 2, right panel) is found in ZnP–[10]CPP⊃Li^+@C_{60}. More detailed data on solvation energies are listed in Table S3.

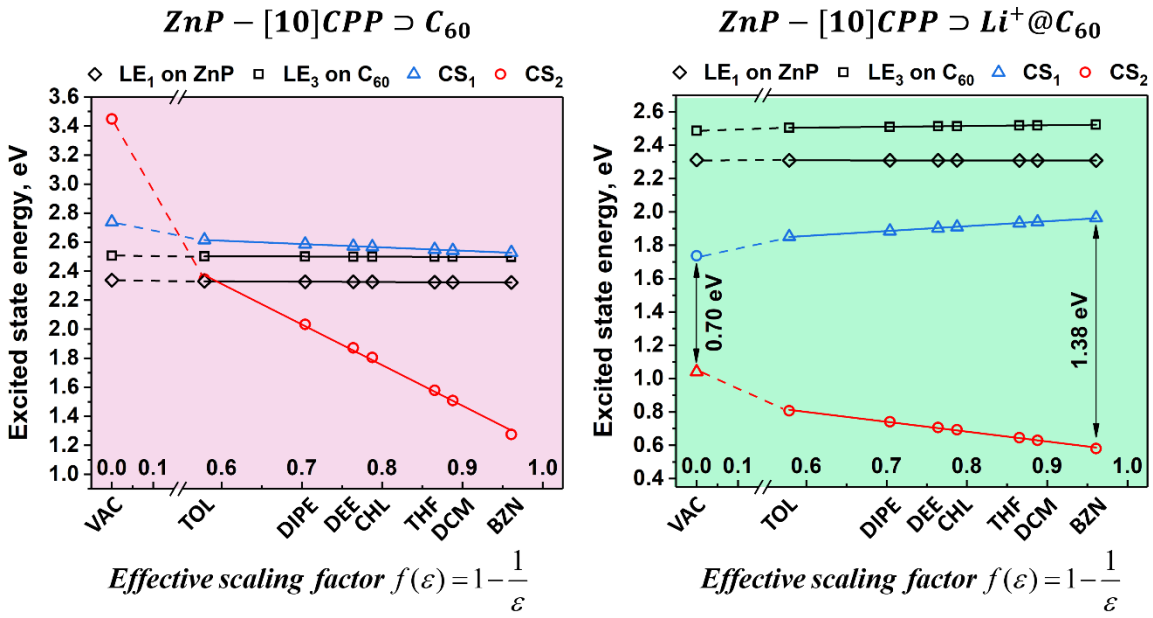

Figure 2. Shift of the LE_1, LE_3, CS_1, and CS_2 states as a function of the effective scaling factor $f(\varepsilon)=\left(1-\frac{1}{\varepsilon}\right)$ for ZnP–[10]CPP⊃C_{60} (left panel) and ZnP–[10]CPP⊃Li^+@C_{60} (right panel) in toluene (TOL), diisopropyl ether (DIPE), diethyl ether (DEE), chloroform (CHL), tetrahydrofuran (THF), dichloromethane (DCM), and benzonitrile (BZN).

Thus, the ZnP–[10]CPP⊃Li^+@C_{60} complex demonstrates a unique combination of CS bands with opposite dependence on medium polarity. Note that the CS_2 band lies in infrared region (IR-B) and its energy varies in the range of 0.81 to 0.59 eV depending on the solvent (Figure 2).

Electron transfer rates.

CS states in the complexes are characterized by weak oscillator strengths and thus have a low probability to be directly populated by light absorption. However, these states can be generated due to their electronic interactions with low-lying LE states. Then, the CS states decay by charge recombination (CR) recovering the ground state. For a better understanding of the excited state properties of the complexes,

we studied the energy transfer (EnT) and singlet-triplet intersystem crossing (ISC) processes. The semi-classical method by Jortner *et al.*[40,41] was used to compute the rates for energy transfer (k_{EnT}), electron transfer (k_{ET}), and charge recombination (k_{CR}). Within this approach, the intramolecular relaxation associated with is ET or EnT is described by an effective vibrational mode, and the rate is controlled by four parameters: electronic coupling of the initial and the final states V_{ij}, the solvation reorganization energy λ_s, the reaction Gibbs energy ΔG^0, and the effective Huang-Rhys factor S_{eff} (for details see the methodological section in SI).

The photophysical study[18] of ZnP-[10]CPP (a precursor for both ZnP–[10]CPP⊃C_{60} and ZnP–[10]CPP⊃Li^+@C_{60}) revealed that its excited state dynamics is dominated by intramolecular energy transfer from [10]CPP to ZnP. When we consider systems containing a fullerene moiety, the LE states on the C_{60} (LE_3 type states) should also be taken into account. To check the possibility of the energy transfer between C_{60} and ZnP, the rate of this process was estimated. For ZnP–[10]CPP⊃C_{60} and ZnP–[10]CPP⊃Li^+@C_{60} in non-polar media, the rate is computed to be $3.97 \cdot 10^1$ s^{-1} and $1.12 \cdot 10^4$ s^{-1}, respectively. Increasing the solvent polarity does not change much the energy transfer rates (see Table 2 and Table S4). The low rate of EnT suggests that this process has no significant effect on the photophysical behavior of the systems.

Since triplet states can also be involved in the photophysics of ZnP–[10]CPP⊃C_{60},[18] we analyzed 10 lowest triplet excited states. In general, the electron density distribution in the triplet states is similar to that in the singlet states. The lowest triplet states resemble closely LE_1 and LE_3. According to our calculations, the lowest triplet LE_3 state in non-polar media is energetically more stable than the singlet CS_2 state. The last state is strongly stabilized in BZN solution in contrast to the triplet LE_3 state, the energy of which is only slightly sensitive to the solvent polarity. Thus, in BZN the singlet CS_2 has a lower energy than the LE_3 triplet Our predictions are consistent with experimental data that indicate a significant role of ISC in photophysics of ZnP–[10]CPP⊃C_{60}. In particular, ISC prevents the formation of CS states in non-polar media, while in

polar solvents it is thermodynamically less favorable than the formation of CS_2. The energy diagram and related data for simulated photoinduced processes in ZnP–[10]CPP⊃C_{60} complex are given in Table S4 and Figure S5.

For the Li^+-doped complex, ISC will not compete with the charge separation because generation of CS_1 and CS_2 singlets from LE_3 is thermodynamically more favorable than singlet-to-triplet conversion of LE_3. Table 2 lists the computed parameters and the rates for EnT, ET, and CR processes for ZnP–[10]CPP⊃Li^+@C_{60} in toluene and benzonitrile. The rate for the processes was computed using an effective frequency of 1600 cm^{-1}. Note that stretching of C=C bonds (1400-1800 cm^{-1}) gives the main contribution to the internal reorganization energy for organic systems including fullerene derivatives. To be on the safe side, we considered the effect of the selected frequency on the rates. As seen from Table S5, the computed ET rates do not change significantly. The diagram in Figure 3 summarizes all studied processes for ZnP–[10]CPP⊃Li^+@C_{60} complex in non-polar (TOL) and polar (BZN) media.

Table 2. Gibbs energy ΔG^0 (in eV), electronic coupling V_{ij} (in eV), solvent reorganization energy λ_s (in eV), Huang-Rhys factor (S_{eff}) and rates (k_X in sec^{-1}) for EnT, CS and CR processes in ZnP–[10]CPP⊃Li^+@C_{60} in non-polar (TOL) and polar (BZN) medium

Type	TOL					BZN				
	$\Delta G^{0[a]}$	$\lvert V_{ij}\rvert$	λ_s	S_{eff}[b]	k_X	ΔG^0	$\lvert V_{ij}\rvert$	λ_s	S_{eff},	k_X
$LE_3 \rightarrow LE_1$	-0.196	$3.64\cdot10^{-7}$	0.001	0.21	$1.12\cdot10^{4}$	-0.215	$3.64\cdot10^{-7}$	0.004	0.21	$4.05\cdot10^{3}$
$LE_3 \rightarrow CS_1$	-0.653	$3.72\cdot10^{-3}$	0.012	1.74	$5.92\cdot10^{10}$	-0.559	$3.72\cdot10^{-3}$	0.221	1.74	$1.84\cdot10^{11}$
$LE_1 \rightarrow CS_2$	-1.502	$4.12\cdot10^{-4}$	0.057	0.60	$2.16\cdot10^{4}$	-1.727	$4.12\cdot10^{-4}$	1.063	0.60	$3.77\cdot10^{8}$
$LE_3 \rightarrow CS_2$	-1.698	$9.37\cdot10^{-4}$	0.057	1.13	$8.23\cdot10^{5}$	-1.942	$9.37\cdot10^{-4}$	1.063	1.13	$1.34\cdot10^{9}$
$CS_1 \rightarrow GS$	-1.852	$1.46\cdot10^{-3}$	0.012	1.47	$6.01\cdot10^{5}$	-1.964	$1.46\cdot10^{-3}$	0.221	1.47	$4.98\cdot10^{6}$
$CS_2 \rightarrow GS$	-0.807	$2.20\cdot10^{-4}$	0.057	0.87	$2.72\cdot10^{7}$	-0.581	$2.20\cdot10^{-4}$	1.063	0.87	$9.79\cdot10^{7}$

[a] Gibbs energy difference between denoted states in corresponding solvent. [b] An effective value of the Huang-Rhys factor $S_{eff} = \lambda_{int} / \hbar\omega_{eff}$, *where* $\hbar\omega_{eff}$ *is set to* $1600\ cm^{-1}$.

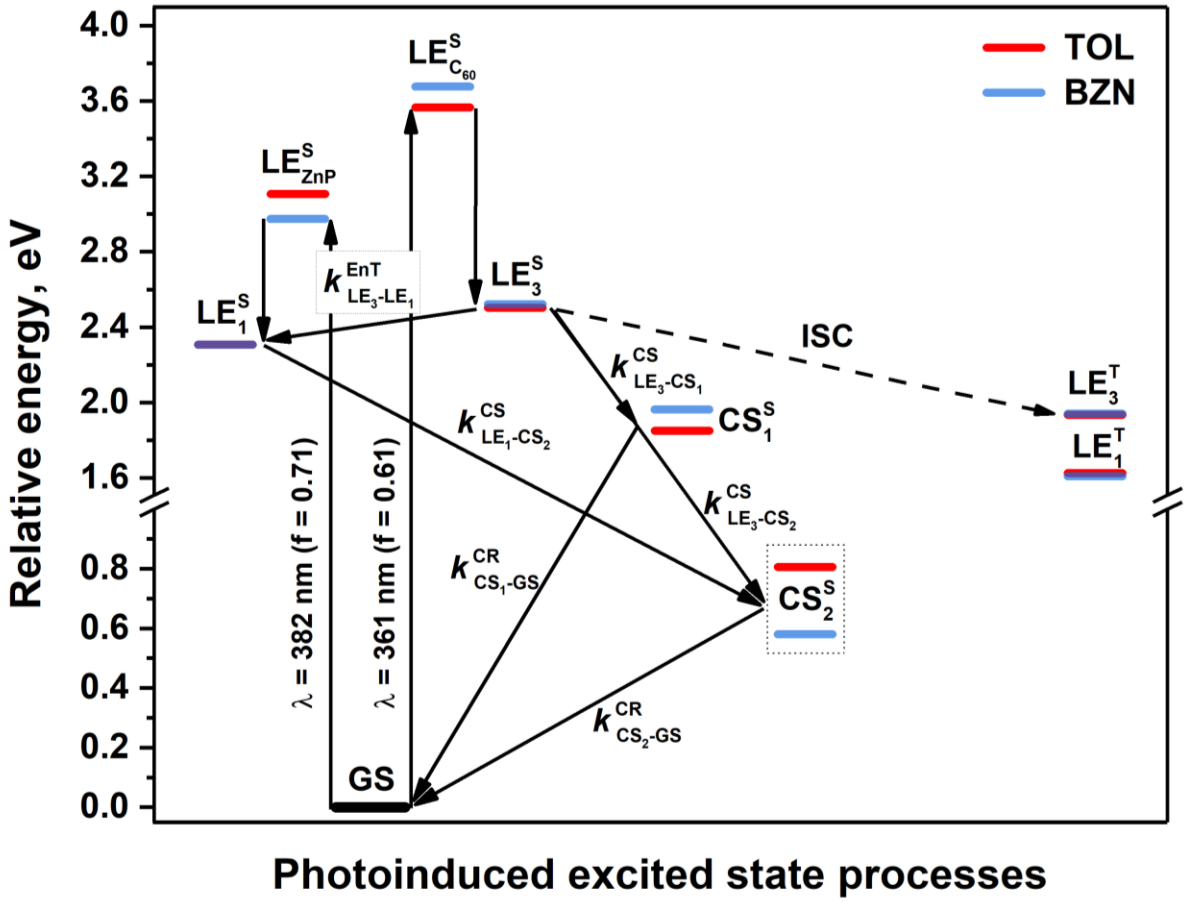

Figure 3. Photoinduced processes in ZnP–[10]CPP⊃Li^+@C_{60} in non-polar toluene solvent (red) and polar benzonitrile (blue) media. Superscripts S and T denote singlet and triplet states.

Charge recombination of CS_1 occurs in the inverted Marcus regime whereas CR of CS_2 is activation less. The CR process for CS_1 is found to be much slower than its generation regardless of the solvent polarity. In the case of CS_2, CR in toluene is significantly faster than generation of this state ($k^{CR}_{CS_2-GS}$ = $2.72\cdot10^7$ *vs* $k^{CS}_{LE_3-CS_2}$ = $8.23\cdot10^5$), and thus the CS_2 state in non-polar media cannot be observed. However in benzonitrile, the rate of the CS_2 formation increases dramatically, while the CR rate changes

insignificantly. This finding suggests that the CS_2 state may play an important role in photophysics of ZnP–[10]CPP⊃Li^+@C_{60} in polar environment.

In conclusion, photoinduced electron transfer processes in ZnP–[10]CPP⊃C_{60} and ZnP–[10]CPP⊃Li^+@C_{60} complexes have been studied in detail using TD-DFT approach. Two types of CS states have been identified (CS_1 and CS_2 are generated by electron transfer from [10]CPP and ZnP units to C_{60}, respectively). In ZnP–[10]CPP⊃C_{60}, only CS_2 state can be populated, whereas generation of the CS_1 states is thermodynamically unfavorable. In contrast, both CS_1 and CS_2 states can be produced by decay of the corresponding LE states in the Li^+-doped complex. The energy transfer from C_{60} to ZnP is found to be quite slow and thus it cannot compete with CS decay. Singlet-triplet intersystem crossing is thermodynamically less favorable than the charge separation reaction. These findings suggest a potential application of ZnP–[10]CPP⊃Li^+@C_{60} in organic photovoltaics. Remarkably, this complex is the first example of a system, where one CS band demonstrates a bathochromic solvent shift, while the other shows a hypsochromic shift which is extremely rarely observed for CS excitations.

Acknowledgments

We are grateful for financial support from the Spanish MINECO (Network RED2018-102815-T, project CTQ2017-85341-P, and Juan de la Cierva formación contract FJCI-2016-29448 to A.J.S. and FJCI-2017-32757 to O.A.S.) and the Catalan DIUE (2017SGR39).

References

(1) Thompson, B. C.; Fréchet, J. M. J. Polymer–Fullerene Composite Solar Cells. *Angew. Chem. Int. Ed.* **2008**, *47*, 58-77.

(2) Bronstein, H.; Nielsen, C. B.; Schroeder, B. C.; McCulloch, I. The role of chemical design in the performance of organic semiconductors. *Nat. Rev. Chem.* **2020**, *4*, 66-77.

(3) Lin, Y.; Li, Y.; Zhan, X. Small molecule semiconductors for high-efficiency organic photovoltaics. *Chem. Soc. Rev.* **2012**, *41*, 4245-4272.

(4) Araki, Y.; Ito, O. Factors controlling lifetimes of photoinduced charge-separated states of fullerene-donor molecular systems. *J. Photochem. Photobiol., C* **2008**, *9*, 93-110.

(5) Gryko, D. T.; Clausen, C.; Roth, K. M.; Dontha, N.; Bocian, D. F.; Kuhr, W. G.; Lindsey, J. S. Synthesis of "Porphyrin-Linker-Thiol" Molecules with Diverse Linkers for Studies of Molecular-Based Information Storage. *J. Org. Chem.* **2000**, *65*, 7345-7355.

(6) Bottari, G.; de la Torre, G.; Guldi, D. M.; Torres, T. Covalent and Noncovalent Phthalocyanine–Carbon Nanostructure Systems: Synthesis, Photoinduced Electron Transfer, and Application to Molecular Photovoltaics. *Chem. Rev.* **2010**, *110*, 6768-6816.

(7) Huang, Q.; Zhuang, G.; Jia, H.; Qian, M.; Cui, S.; Yang, S.; Du, P. Photoconductive Curved-Nanographene/Fullerene Supramolecular Heterojunctions. *Angew. Chem. Int. Ed.* **2019**, *58*, 6244-6249.

(8) Murthy, C. N.; Geckeler, K. E. The water-soluble β-cyclodextrin–[60]fullerene complex. *Chem. Commun.* **2001**, 1194-1195.

(9) Liu, J.; Alvarez, J.; Ong, W.; Kaifer, A. E. Network Aggregates Formed by C60 and Gold Nanoparticles Capped with γ-Cyclodextrin Hosts. *Nano Lett.* **2001**, *1*, 57-60.

(10) Zhang, W.; Gong, X.; Liu, C.; Piao, Y.; Sun, Y.; Diao, G. Water-soluble inclusion complex of fullerene with γ-cyclodextrin polymer for photodynamic therapy. *J. Mater. Chem. B* **2014**, *2*, 5107-5115.

(11) Bourdelande, J. L.; Font, J.; González-Moreno, R.; Nonell, S. Inclusion complex of calix[8] arene-C60: photophysical properties and its behaviour as singlet molecular oxygen sensitiser in the solid state. *J. Photochem. Photobiol., A* **1998**, *115*, 69-71.

(12) Bhattacharya, S.; Nayak, S. K.; Chattopadhyay, S.; Banerjee, M.; Mukherjee, A. K. Spectrophotometric and thermodynamic study of supramolecular complexes of [60]- and [70]fullerenes with a number of calix[n]arenes. *J. Chem. Soc., Perkin Trans. 2* **2001**, 2292-2297.

(13) Iwamoto, T.; Watanabe, Y.; Sakamoto, Y.; Suzuki, T.; Yamago, S. Selective and Random Syntheses of [n]Cycloparaphenylenes (n = 8–13) and Size Dependence of Their Electronic Properties. *J. Am. Chem. Soc.***2011**, *133*, 8354-8361.

(14) Lewis, S. E. Cycloparaphenylenes and related nanohoops. *Chem. Soc. Rev.* **2015**, *44*, 2221-2304.

(15) Lu, D.; Huang, Q.; Wang, S.; Wang, J.; Huang, P.; Du, P. The Supramolecular Chemistry of Cycloparaphenylenes and Their Analogs. *Front. Chem.* **2019**, *7*, 668.

(16) Wu, D.; Cheng, W.; Ban, X.; Xia, J. Cycloparaphenylenes (CPPs): An Overview of Synthesis, Properties, and Potential Applications. *Asian J. Org. Chem.* **2018**, *7*, 2161-2181.

(17) Omachi, H.; Matsuura, S.; Segawa, Y.; Itami, K. A Modular and Size-Selective Synthesis of [n]Cycloparaphenylenes: A Step toward the Selective Synthesis of [n,n] Single-Walled Carbon Nanotubes. *Angew. Chem. Int. Ed.* **2010**, *49*, 10202-10205.

(18) Xu, Y.; Wang, B.; Kaur, R.; Minameyer, M. B.; Bothe, M.; Drewello, T.; Guldi, D. M.; von Delius, M. A Supramolecular [10]CPP Junction Enables Efficient Electron Transfer in Modular Porphyrin–[10]CPP⊃Fullerene Complexes. *Angew. Chem. Int. Ed.* **2018**, *57*, 11549-11553.

(19) Kc, C. B.; D'Souza, F. Design and photochemical study of supramolecular donor–acceptor systems assembled via metal–ligand axial coordination. *Coord. Chem. Rev.* **2016**, *322*, 104-141.

(20) Nierengarten, J.-F. Weak Intramolecular Interactions to Stabilize Supramolecular Fullerene-Porphyrin Conjugates and to Control the Conformation of Multiporphyrinic Arrays. *Eur. J. Inorg. Chem.* **2019**, *2019*, 4865-4878.

(21) Moreira, L.; Calbo, J.; Aragó, J.; Illescas, B. M.; Nierengarten, I.; Delavaux-Nicot, B.; Ortí, E.; Martín, N.; Nierengarten, J.-F. Conjugated Porphyrin Dimers: Cooperative Effects and Electronic Communication in Supramolecular Ensembles with C60. *J. Am. Chem. Soc.***2016**, *138*, 15359-15367.

(22) Yamamoto, M.; Föhlinger, J.; Petersson, J.; Hammarström, L.; Imahori, H. A Ruthenium Complex–Porphyrin–Fullerene-Linked Molecular Pentad as an Integrative Photosynthetic Model. *Angew. Chem. Int. Ed.* **2017**, *56*, 3329-3333.

(23) Wolf, M.; Herrmann, A.; Hirsch, A.; Guldi, D. M. Rigid, Branched Porphyrin Antennas: Control over Cascades of Unidirectional Energy Funneling and Charge Transfer. *J. Am. Chem. Soc.* **2017**, *139*, 11779-11788.

(24) Stasyuk, A. J.; Stasyuk, O. A.; Solà, M.; Voityuk, A. A. Peculiar Photoinduced Electron Transfer in Porphyrin–Fullerene Akamptisomers. *Chem. - Eur. J.* **2019**, *25*, 2577-2585.

(25) Ueno, H.; Nishihara, T.; Segawa, Y.; Itami, K. Cycloparaphenylene-Based Ionic Donor–Acceptor Supramolecule: Isolation and Characterization of Li+@C60⊂[10]CPP. *Angew. Chem. Int. Ed.* **2015**, *54*, 3707-3711.

(26) Becke, A. D. Density-functional exchange-energy approximation with correct asymptotic behavior. *Phys. Rev. A* **1988**, *38*, 3098-3100.

(27) Lee, C.; Yang, W.; Parr, R. G. Development of the Colle-Salvetti correlation-energy formula into a functional of the electron density. *Phys. Rev. B* **1988**, *37*, 785-789.

(28) Weigend, F.; Ahlrichs, R. Balanced basis sets of split valence, triple zeta valence and quadruple zeta valence quality for H to Rn: Design and assessment of accuracy. *Phys. Chem. Chem. Phys.* **2005**, *7*, 3297-3305.

(29) Yanai, T.; Tew, D. P.; Handy, N. C. A new hybrid exchange–correlation functional using the Coulomb-attenuating method (CAM-B3LYP). *Chem. Phys. Lett.* **2004**, *393*, 51-57.

(30) Hashmi, M. A.; Lein, M. Carbon Nano-onions as Photosensitizers: Stacking-Induced Red-Shift. *J. Phys. Chem. C* **2018**, *122*, 2422-2431.

(31) Stasyuk, A. J.; Stasyuk, O. A.; Solà, M.; Voityuk, A. A. Photoinduced Charge Shift in Li+-Doped Giant Nested Fullerenes. *J. Phys. Chem. C* **2019**, *123*, 16525-16532.

(32) Stasyuk, A. J.; Stasyuk, O. A.; Solà, M.; Voityuk, A. A. Hypsochromic solvent shift of the charge separation band in ionic donor–acceptor Li+@C60⊂[10]CPP. *Chem. Commun.* **2019**, *55*, 11195-11198.

(33) Mennucci, B. Polarizable continuum model. *WIREs Comput. Mol. Sci.* **2012**, *2*, 386-404.

(34) Stasyuk, A. J.; Stasyuk, O. A.; Filippone, S.; Martin, N.; Solà, M.; Voityuk, A. A. Stereocontrolled Photoinduced Electron Transfer in Metal-Fullerene Hybrids. *Chem. - Eur. J.* **2018**, *24*, 13020-13025.

(35) Izquierdo, M.; Platzer, B.; Stasyuk, A. J.; Stasyuk, O. A.; Voityuk, A. A.; Cuesta, S.; Solà, M.; Guldi, D. M.; Martín, N. All-Fullerene Electron Donor–Acceptor Conjugates. *Angew. Chem. Int. Ed.* **2019**, *58*, 6932-6937.

(36) Stasyuk, A. J.; Stasyuk, O. A.; Solà, M.; Voityuk, A. A. Photoinduced electron transfer and unusual environmental effects in fullerene–Zn-porphyrin–BODIPY triads. *Phys. Chem. Chem. Phys.* **2019**, *21*, 25098-25107.

(37) Kavarnos, G. J.; Turro, N. J. Photosensitization by reversible electron transfer: theories, experimental evidence, and examples. *Chem. Rev.* **1986**, *86*, 401-449.

(38) Guldi, D. M.; Prato, M. Excited-State Properties of C60 Fullerene Derivatives. *Acc. Chem. Res.* **2000**, *33*, 695-703.

(39) El-Khouly, M. E.; Ito, O.; Smith, P. M.; D'Souza, F. Intermolecular and supramolecular photoinduced electron transfer processes of fullerene–porphyrin/phthalocyanine systems. *J. Photochem. Photobiol., C* **2004**, *5*, 79-104.

(40) Ulstrup, J.; Jortner, J. The effect of intramolecular quantum modes on free energy relationships for electron transfer reactions. *J. Chem. Phys.* **1975**, *63*, 4358-4368.

(41) Jortner, J. Temperature dependent activation energy for electron transfer between biological molecules. *J. Chem. Phys.* **1976**, *64*, 4860-4867.